A Small-Angle Neutron Scattering Study of Cholic Acid-Based Organogel Systems

Hendra M. Willemen,[†] Antonius T. M. Marcelis,*[,†] Ernst J. R. Sudhölter,[†] Wim G. Bouwman,[‡] Bruno Demé,[§] and Pierre Terech[||]

Laboratory of Organic Chemistry, Wageningen University, Dreijenplein 8, 6703 HB, The Netherlands; Interfacultair Reactor Instituut, Delft University of Technology, Mekelweg 15, 2629 JB Delft, The Netherlands; Institute Laue-Langevin, 6, rue Jules Horowitz BP 156-38042 Grenoble Cedex 9, France; and Laboratoire Physico-Chimie Moléculaire, UMR 5819 CEA-CNRS-Université J. Fourier, Département de Recherche Fondamentale sur la Matière Condensée, C. E. A.-Grenoble, 17, Rue des Martyrs, 38054 Grenoble Cedex 09, France

Received June 13, 2003. In Final Form: November 6, 2003

Small-angle neutron scattering measurements were performed on some cholic acid-based gel systems in order to gain detailed information about the network structure. The presence of thin fibers with a radius of about 10−20 Å was found for various gelators. Two types of interaction between different sorts of fibers were demonstrated, depending on the molecular structure of the gelator. The first type involves the presence of microcrystalline knots with a dimension of about 100−200 Å between the fibers. Upon heating, this network gradually disintegrates. The second type involves loose entanglements between flattened fibers. The occurrence of these types of interaction is related to the length of the alkyl tail attached to cholic acid.

Introduction

Research in the field of organogels has received more and more attention over the last several years, and the number of low molecular mass organogelators is rapidly growing.[1−4] The gelling capability of these compounds is not yet understood in detail, but one important requirement is the ability of the gelator molecules to spontaneously form aggregates, which encapsulate the solvent in a three-dimensional network. For many organogelators, the gel network consists of fibers, which in turn assemble into larger aggregates. Aggregation of low molecular mass organogelators is usually driven by specific noncovalent intermolecular forces, such as hydrogen-bond formation, metal coordination bond formation, hydrophobic interactions, dipole−dipole interactions, or van der Waals interactions.

A large number of organogelators are based on steroids such as cholesterol in which the gelation is driven by hydrophobic interactions.[5] Hydrogen-bond interactions are important in gelation of bile steroids such as cholic acid, especially when amide groups are present.[6−11]

We found that several compounds in which cholic acid is coupled to an α-amino acid ester act as gelators for aromatic solvents, producing transparent and stable gels.[6] Other cholic acid amides were also found to act as organogelators for aromatic solvents.[7] Although gelators of various molecular structures were used, the hydrogen-bonded aggregation mode and corresponding molecular requirements for gelation are similar. Also, the macroscopic properties of the gels, such as transparency and stability, seem equal. Electron microscopy (EM) studies revealed some differences between the network of the different organogelators. Electron microscopy (EM) images for *N*-octadecylcholamide (C18) in benzene show thin, almost monomolecular fibers.[6] For another type of gelator, i.e., *N*-cholyl D-leucine methyl ester (D-LeuMe) in benzene, EM images show thicker fibers,[7] but these could also be interpreted as bundles of fibers. However, detailed information about the network structure and its dimensions is lacking.

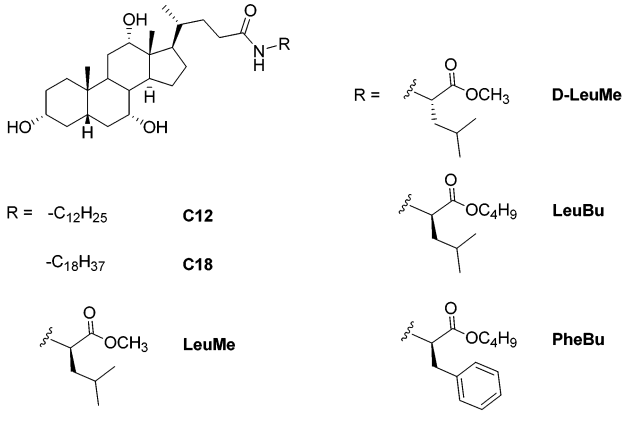

A suitable method to obtain this kind of information is small-angle neutron scattering (SANS).[12] A number of

* Corresponding author. E-mail: ton.marcelis@wur.nl.
[†] Wageningen University.
[‡] Delft University of Technology.
[§] Institut Laue-Langevin.
[||] Laboratoire Physico-Chimie Moléculaire.

(1) Gronwald, O.; Snip, E.; Shinkai, S. *Curr. Opin. Colloid Interface Sci.* **2002**, *7*, 148−156.
(2) Terech, P.; Weiss, R. G. *Chem. Rev.* **1997**, *97*, 3133−3159.
(3) Abdallah, D. J.; Weiss, R. G. *Adv. Mater.* **2000**, *12*, 1237−1247.
(4) Special issue of *Langmuir* **2002**, *18* (19): Self-Assembled Fibrillar Networks.
(5) Geiger, G.; Stanescu, M.; Chen, L.; Whitten, D. G. *Langmuir* **1999**, *15*, 2241−2245.
(6) Willemen, H. M.; Vermonden, T.; Marcelis, A. T. M.; Sudhölter, E. J. R. *Eur. J. Org. Chem.* **2001**, 2329−2335.
(7) Willemen, H. M.; Vermonden, T.; Marcelis, A. T. M.; Sudhölter, E. J. R. *Langmuir* **2002**, *18*, 7102−7106.
(8) Hishikawa, Y.; Sada, K.; Watanabe, R.; Miyata, M.; Hanabusa, K. *Chem. Lett.* **1998**, 795−796.
(9) Nakano, K.; Hishikawa, Y.; Sada, K.; Miyata, M.; Hanabusa, K. *Chem. Lett.* **2000**, 1170−1171.
(10) Maitra, U.; Kumar, P. V.; Chandra, N.; D'Souza, L. J.; Prasanna, M. D.; Raju, A. R. *Chem. Commun.* **1999**, 595−596.
(11) Sangeetha, N. M.; Balasubramanian, R.; Maitra, U.; Ghosh, S.; Raju, A. R. *Langmuir* **2002**, *18*, 7154−7157.

10.1021/la035041y CCC: $27.50
Published on Web 01/31/2004

organogelators have already been studied with SANS.[13−19] Therefore, different cholic acid-based organogelators were studied that were previously obtained in order to acquire information about the structure and dimensions of the single fibers and the fiber−fiber interactions in the gel network of the different gelators. In this way, differences on (sub)microscopic level can be revealed. Furthermore, possible structural changes in the LeuMe gel network as a function of temperature were investigated.

Experimental Section

The synthesis and characterization of the compounds were previously described.[6,7] Benzene-d_6 (99.6% D) of p.a. quality was purchased from Aldrich. Gels were prepared by heating and subsequently cooling a solution of gelator in deuterated benzene in different concentrations. A grain of molecular sieve (4 Å) was added to the prepared gels, to ensure they were anhydrous before the measurement.

SANS measurements were performed at the 58 MW reactor at Institut Laue-Langevin (ILL) in Grenoble, France at the D11 facility. The wavelength of the collimated neutron beam was 6 Å. Every sample was measured with a ^{3}He gas detector (CERCA) of 64 × 64 cm^2 at three distances: 1.1, 4, and 20 m. The investigated Q range was 0.002−0.3 Å^{-1}. The wavelength spread was about 10%. Samples in 1 mm pathway quartz cuvettes were placed in a sample holder, kept at constant temperature around 27 °C, unless stated otherwise. Corrections for background and transmission were applied. Background measurements consisted of empty cell and benzene-d_6. Measurement of H_2O was used to correct for the detector efficiency, and calibration was done using direct beam measurements. The scattered intensity was corrected for background and parasitic scattering, placed on an absolute level using a direct measurement of the beam flux, and circularly averaged to yield the scattered intensity, $I(q)$, as a function of the wave vector, q, where $q = (4\pi/\lambda)\sin(\theta/2)$ (λ is the wavelength of the neutrons and θ is the scattering angle).

Results and Discussion

Plots of the scattering cross section $I(Q)$ as a function of momentum transfer Q were obtained for the various gels. An example for gels with different concentrations of compound LeuMe is shown in Figure 1 with logarithmic scales.

As we can see, the scattered intensity increases with concentration, because the amount of scattering material increases. A dynamic range of nearly 6 orders of magnitude is obtained: from little below 0.001 cm^{-1} to almost 500 cm^{-1}.

These gel systems are extremely sensitive to water, because the structure is based on hydrogen bonds.[20] Although we tried to shield the gels from the environment, we found that in some cases water diffused from the air into the samples during measurements, due to the high humidity of the air during the days of the experiments. This resulted in a diminished rigidity of the gel during the measurement for some samples and discontinuities in the $I(Q)$ vs Q plots. These measurements were not included in the further analysis.

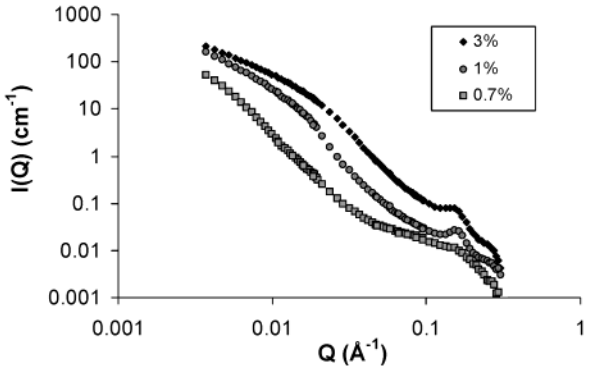

Figure 1. Scattering cross section at various concentrations of LeuMe.

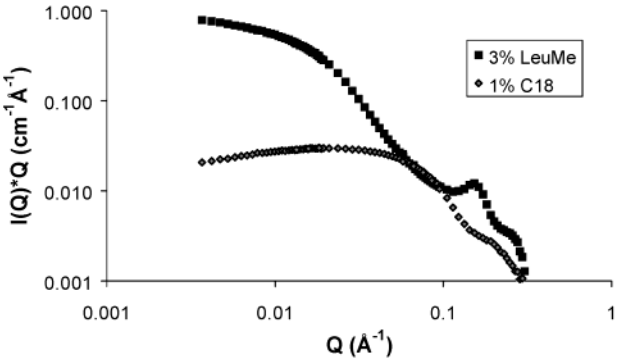

Figure 2. Scattering cross section showing the fiberlike structure for 1% C18 and 3% LeuMe.

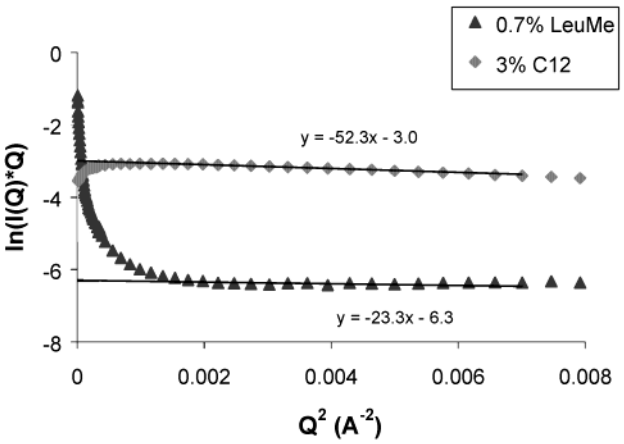

Figure 3. Guinier plots for rodlike particles of 3% C12 and 0.7% LeuMe.

We assume that there is a critical concentration, below which no aggregation takes place. Therefore, we have to keep in mind that part of the material is not contributing to the gel network, but is freely dissolved, and that the actual volume fraction of scatterers is lower than the added volume fraction. Furthermore, we do not know the exact density (δ) of the materials. For calculations, we assume it equals 1 g/mL.

More useful ways to plot SANS results are shown in Figures 2 and 3. From a plot of the product of $I(Q)$ and Q vs Q, both on a logarithmic scale, information can be gained from different Q ranges. If there is a plateau followed by a q^{-1} power law decay in the middle-Q range, this usually indicates the presence of fibers. For most of our systems we find curves with a plateau and q^{-1} decay, but there are

(12) For an introduction to SANS: King, S. M. Small-Angle Neutron Scattering. In *Modern Techniques for Polymer Characterisation*; Pethrick, R. A., Dawkins, J. V., Eds; Wiley: Chichester, 1999; Chapter 7, pp 171−232.
(13) Terech, P.; Coutin, A.; Giroud-Godquin, A. M. *J. Phys. Chem. B* **1997**, *101*, 6810−6818.
(14) Terech, P. *Prog. Colloid Polym. Sci.* **1996**, *102*, 64−70.
(15) Terech, P. *Ber. Bunsen-Ges. Phys. Chem.* **1998**, *102*, 1630−1643.
(16) Terech, P.; Pasquier, D.; Bordas, V.; Rossat, C. *Langmuir* **2000**, *16*, 4485−4494.
(17) Imae, T.; Hayashi, N.; Matsumoto, T.; Tada, T.; Furusaka, M. *J. Colloid Interface Sci* **2000**, *225*, 285−290.
(18) Fukuda, H.; Goto, A.; Imae, T. *Langmuir* **2002**, *18*, 7107−7114.
(19) Schmidt, R.; Schmutz, M.; Mathis, A.; Decher, G.; Rawiso, M.; Mésini, P. J. *Langmuir* **2002**, *18*, 7167−7173.
(20) Tamaru, S.; Luboradzki, R.; Shinkai, S. *Chem. Lett.* **2001**, 336−337.

Table 1. Radii Derived from the Guinier Plots[a]

compd	concn (wt %)	radius calcd from slope (Å)	compd	concn (wt %)	radius calcd from slope (Å)
C12	0.5	18.2	D-LeuMe	1	*a*
	3	14.5	LeuBu	3	13.8
C18	1	21.7	PheBu	3	9.8
LeuMe	0.7	9.6		10	2.5
	1	*a*			
	3	*a*			

[a] Condition $rQ < 1$ not met.

some deviations. Two typical examples are shown in Figure 2. For the plot of C18 we find a "bump", instead of a plateau. This was also found for compounds C12, LeuBu, and PheBu. In the plot of compound LeuMe, we see a Bragg peak in the large-Q range. Such a Bragg peak was also found in the plots of D-LeuMe, but not in any other plots.

The second way is a plot of $\ln[I(Q)Q]$ vs Q^2, which is presented in Figure 3 for 3% C12 and 0.7% LeuMe. For most compounds a straight line with negative slope was found in the low-Q range, a so-called Guinier plot for fibers. From these lines the radius r can be derived, assuming rodlike scatterers, using the Guinier approximation[13]

$$I(Q) = \{\phi(\pi r \Delta\rho)^2/Q\} \exp(-Q^2r^2/4)$$

in which ϕ is the volume fraction. Now the radius can be determined from the slope of the Guinier plot. The Guinier equation is only valid in the low-Q range, so the calculated values must meet the condition $rQ < 1$ in order to be considered reliable. The results are summarized in Table 1.

In principle, the radii can also be obtained from the intercept at $Q = 0$. However, this value will be lower than the one obtained from the slope, because the volume fraction is included in this method. As mentioned before, there is an unknown critical aggregation concentration, which we have to consider. The amount of gelator in the fibers is always lower than the total amount added. So the calculated radius from the intercept will be smaller than the actual value. Higher concentrations of gelator will give rise to extra scattering that will affect the form factor analysis. This also means that the radii obtained from the higher concentrations are less accurate than those obtained from the lower concentrations.

Generally, the radius of the fibers for all present compounds is about 10−20 Å. This means that the fibers are practically monomolecular in thickness. For example, these calculations give a fiber radius of about 16 Å, and thus a mean diameter of 32 Å for C12. This molecule in a fully stretched conformation has a length of about 30 Å, so the diameter of the fibers corresponds very well with the molecular length. Presumably, the steroid parts of these molecules are stacked in the center of a fiber, and the alkyl tails are located around the center, pointing outward. One can envisage that the alkyl tails are not completely stretched and assume some gauche conformations, due to interactions with the surrounding solvent. Compared to many other gelators, the fibers from these cholic acid derivatives are very thin. This could also explain the transparency of these gels. It also means that the obtained values are close to the lower limit of what can be measured with SANS. Recently, some other gel systems were described with very thin fibers. For example, hydrogen-bonded gels from bis-urea organogelators were found to consist of fibers with diameters of about 26 Å,[21] and a water-soluble dye was found to give fibrils with a diameter of about 40 Å.[22]

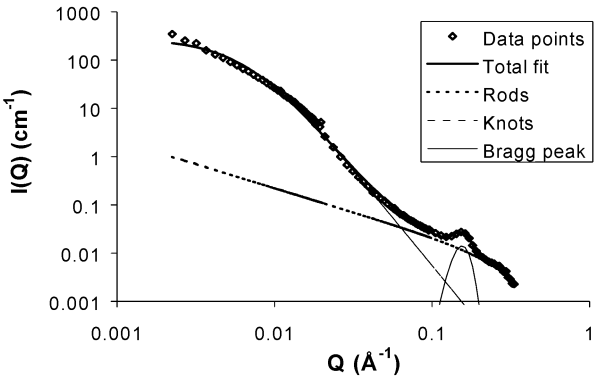

Figure 4. Fit of the scattering cross section of 1% LeuMe with cylindrical fibers with crystalline knots.

From the different plots we can also get information about the way single fibers interact with each other. When we look in some more detail at the plots of $I(Q)Q$ vs Q and $\ln[I(Q)Q]$ vs Q^2 for all gelators, we see that there are generally two types of interactions in which the fibers are connected to each other, micocrystalline knots or entangled interactions. Both types are common among organogelators.[14,15]

Microcrystalline Knots. This first type of interaction is found for the gelators LeuMe and D-LeuMe. In the plots of $I(Q)Q$ vs Q a typical middle-Q range decay is found, which indicates the presence of rodlike scatterers. This is shown for LeuMe in Figure 2. However, a remarkable feature in these plots is a clear Bragg peak at $Q = 0.155$ Å^{-1}. A Bragg peak indicates the presence of crystalline packing in at least part of the structure. Probably the gel consists of fibers that occasionally join and form microcrystalline junction zones, or knots, and thus form a network. The repeating unit inside the knots has dimension $d = 2\pi/0.155 = \sim 40$ Å. The average diameter of the knots can be estimated from the full width at half-height of the Bragg peak; this is about 0.06 Å^{-1}. This corresponds roughly to an average size of $2\pi/0.06 = \sim 100$ Å. So each knot contains only about three repeating units in length. There is a feature in the Guinier plots, shown in Figure 3, that confirms the presence of crystalline knots. At very low Q values a drastic increase in the scattering cross section is found, as a result of these crystalline knots. This increase has a considerable influence on the Guinier plot, and it complicates the derivation of the fiber radius.

A more quantitative analysis of these measurements is done. We have focused on modeling the scattering curves for LeuMe. A model was used that described the network structure of the gel as a mixture of round, rodlike fibers and microcrystalline knots. In Figure 4 a modeled fit for 1% LeuMe is displayed, together with the experimental curve. The fit is the sum of three separate contributions, which are also shown individually: the cylinder-like fibers, I_{cyl}; the knots, I_{knot}; and the Bragg peak, I_{Bragg}. Generally, at low-Q range the largest contribution comes from the knots, at middle-Q range from the rods, and at high-Q range from the Bragg peak, which is again caused by the crystalline knots. The knots are described with the Debye−Bueche formula[13]

(21) Lortie, F.; Boileau, S.; Bouteiller, L.; Chassenieux, C.; Demé, B.; Ducouret, G.; Jalabert, M.; Lauprêtre, F.; Terech, P. *Langmuir* **2002**, *18*, 7218−7222.

(22) Imae, T.; Gagel, L.; Tunich, C.; Platz, G.; Iwamoto, T., Funayama, K. *Langmuir* **1998**, *14*, 2197−2200.

$$I_{knot}(Q) = 8\pi\phi_{knot}(1 - \phi_{knots})(\Delta\rho)^2 d^3/(1 + d^2Q^2)^2$$

in which ϕ_{knot} is the volume fraction of material in the knots and d is the average size of the knots. Since this equation is only significant in the low-Q region, any other model for a 3D particle with a radius could be used. The radius is the only significant parameter. It was not possible to fit the low-Q bump with a cylinder model with a larger diameter. The knots do not have one particular shape but are defined as an exponentially decreasing density. One cannot see the Q^{-4} decay at higher Q values, since the other scattering components obscure this tail. The cylinder-like fibers are described with the equation[23]

$$I_{cyl}(Q) = (\phi_{cyl}/2Qr^2)\,[A\Delta\rho(2J_1(Qr))/Qr]^2$$

in which ϕ_{cyl} is the volume fraction of material in the rods, A is the cross-sectional area of a rod, and J_1 is the Bessel function of the first kind ($A\Delta\rho$ gives the scattering length per unit length). The Bragg peak is described with a Gaussian equation with certain position, amplitude, and width.

Parameters describing the dimensions of the network in the model were varied to obtain the best possible fit. In Table 2 the resulting data are shown for fits of LeuMe at different concentrations. There is some variation in the values obtained between the different concentrations, but they do give a general impression about the order of magnitude for the obtained values. The radius of the rods is about 10 Å and the average diameter of the knots is about 180 Å. The knot size seems to decrease with concentration. These data are on the same order of magnitude as the results calculated directly from the width of the Bragg peak.

For LeuMe, temperature-dependent measurements were performed to study the gel structure upon melting. In Figure 5 the curves of a 3% gel of LeuMe are shown for three different temperatures. They show a decrease of scattered intensity at higher temperature. At 37 °C there is mostly a decrease in the scattering intensity at low-Q values.

The plot still shows the typical features for rodlike scatterers: a plateau followed by decay in the middle-Q range. Also the radius that can be calculated from the Guinier plot has about the same value as the radius calculated for lower temperature. However, the Bragg peak in the scattering plot is much smaller. This could indicate that the crystalline knots disintegrate first, while the fibers are still intact. At 59 °C there is no scattering left at all, meaning that also the fibers have disintegrated and a solution is present. A gradual breakdown of the gel network agrees well with our earlier suggestion that a partial melting of the gel occurs.[6] This was based on DSC measurements, where we found a broad peak in the DSC curve before the actual melting of the gel occurred.

Entangled Interactions. This second type of interaction between the fibers is found for the gelators C12, C18, LeuBu, and PheBu. In the plots of $I(Q)Q$ vs Q, there is not a plateau followed by a decay or only a decay, but in the lower Q range, there is a "bump". This is shown for C18 in Figure 2, and it indicates a strong interaction between the fibers. However, this interaction does not involve distinct knots, but more loose entanglements. Although SANS gives no information about the dynamics of the system, we assume these are transient entanglements. Also the Guinier plots show a remarkable feature. At very small Q values a decreased intensity is observed, as shown for C12 in Figure 3. This could be a signature of the structure factor describing correlation between the fibers. This observation supports the idea of entangled interactions between the fibers.

(23) Adapted from ref 13.

Table 2. Data from Modeled Fits for the Curves of LeuMe Shown in Figure 1

concn (wt %)	fiber radius (Å)	knot size (Å)
0.7	10.3 ± 1.0	300 ± 50
1	6.4 ± 1.0	150 ± 40
3	9.5 ± 1.0	90 ± 30

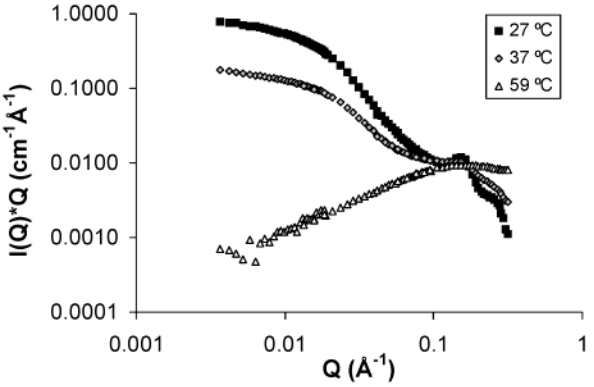

Figure 5. Scattering cross section for 3% LeuMe at various temperatures.

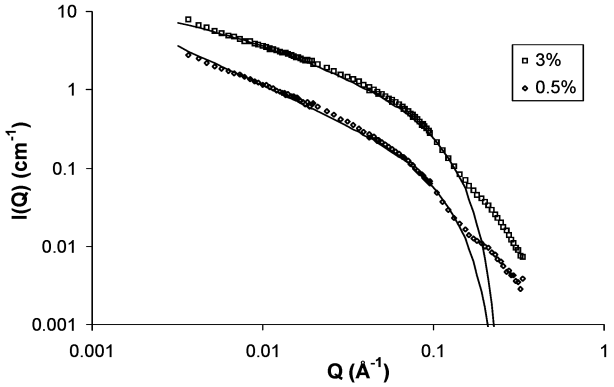

Figure 6. Calculated fits (solid lines) for C12 with cylindrical fibers at two different concentrations.

Effort was made to model the experimental scattering curves for a compound with this type of interaction. However, we did not yet succeed in giving a full quantitative description of the measurements. Using the so-called random phase approximation the low-angle part of the scattering curve can be described effectively, as can be seen in Figure 6 for C12 at two different concentrations. The scattering for rodlike scatterers was expressed in the function $I(Q)$ in the same way as above. To take the interactions between the fibers into account, the scattering cross section for correlated rods [$I_{struc}(Q)$] was expressed using the random phase approximation[24]

$$I_{struc}(Q) \propto I(Q)/[1 + \nu I(Q)]$$

in which ν is proportional to the concentration of the cylinders. The scattering curve of C12 with a concentration of 0.5 wt % could be well-described with only isolated rods

(24) For a review on analytical models for the interpretation of SANS data, see: Pedersen, J. S. *Adv. Colloid Interface Sci.* **1997**, *70*, 171–210.

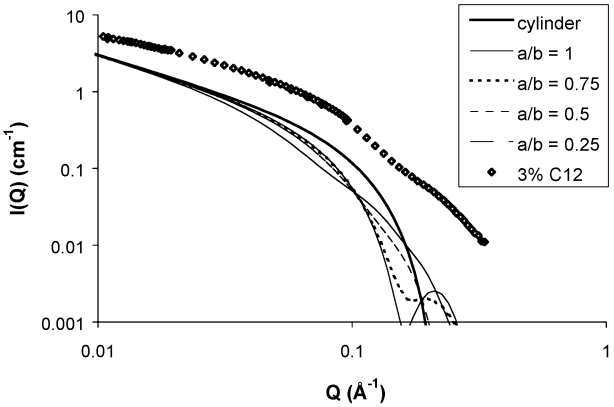

Figure 7. Calculated scattering cross section for cylindrical fibers and for rectangular fibers with different aspect ratios and the experimental data for 3% C12. The experimental data have been shifted with respect to the theoretical curves.

with a radius of 18.2 Å, as determined with the Guinier analysis. To have a good description of the data it was necessary to assume that a fraction of 0.3 of the material is present in the fibers. The fit is satisfactory up till a momentum transfer of about 0.1 Å^{-1}. For the scattering curve with a concentration of 3 wt % it was necessary to take correlations into account. A good description of the data in the same Q range was obtained with a value of 0.1 for ν. A fraction of 0.2 of the added material was present in the scattering fibers. The discrepancies in the fit were again found for Q larger than 0.1 Å^{-1}. Thereafter, the measured intensity is higher than the calculated intensity. There is a small bump visible at high Q values that is not described with this model.

The discrepancy between measured and modeled curves for all concentrations of C12 at high Q value could indicate that a description with round fibers is not appropriate and that another cross section for the fibers is more suited. So calculations were performed assuming the presence of rectangular fibers. In Figure 7 modeled curves are shown for cylindrical fibers and for rectangular fibers with different values for the aspect ratio a/b in which a and b represent half the sides of the rectangular cross section. These calculations do not fit a particular data set but are meant to give a general picture. For comparison, experimental data for 3% C12 are shown. The rectangular model was described using the following equation[25,26]

$$I(Q) = (2\phi_{rod}/Q)\Delta\rho^2 A \int_0^{\pi/2}[\{\sin(Qa \sin \varphi) \sin (Qb \cos \varphi)\}/\{Qa \sin \varphi\ Qb \cos \varphi\}]^2 \, d\varphi$$

in which $\Delta\rho$ is the specific neutron contrast of the fiber, and A is the cross-sectional area of the fiber. For these calculations a 10% spread in wavelength was taken into account. In the low-Q range, there is little difference between this model and the model described above for round fibers. However, for Q larger than 0.1 Å^{-1} this rectangular fiber model seems to fit the experimental data better. Especially the curves with aspect ratios of 0.25 and 0.5 seem to give a rather good resemblance to the experimental curve. The intensity at the bump is, however, higher in the measurement than in the models, which indicates that internal structure in the cross section of the fibers is present. We did not attempt to further model this effect. A description with a range of length distributions did not work. Even short rods did not yield this bump at the high Q values.

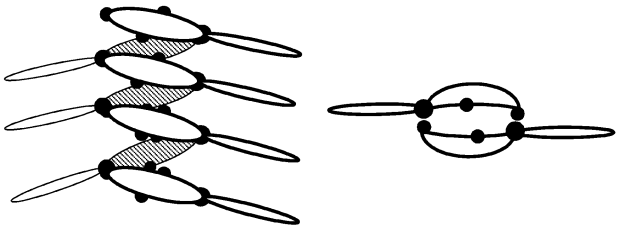

Figure 8. Schematic representation of possible fiber model for compound C12: side view (left) and top view (right); • = hydroxyl group; ● = amide group.

This rectangular shape of fiber is found for the gels of compounds C12, C18, LeuBu, and PheBu. They all show a similar curve with a characteristic, small bump at high Q value (above 0.1 Å^{-1}). Actually, from these calculations it cannot be concluded that the fibers are rectangular-shaped. They might as well be elliptical-shaped. What can be concluded is that these gelators form flattened fibers, probably with an aspect ratio of about 0.5 or lower.

Besides a difference in the interactions between the fibers of the various cholic acid-based gels, there is also a difference in the shape of the single fibers that are formed. One group of gelators forms a network of round fibers that connect by means of microcrystalline knots. A second group of gelators forms a network of flat fibers with loose entanglements. Comparing the molecular structures from the gelators in these two groups, a possible trend can be seen. In the group with the entangled flat fibers, all compounds contain an alkyl tail of at least four carbon atoms, which is attached directly to cholic acid or via an amino acid. On the other hand, in the group with the knotted, round fibers, the compounds contain only a methyl group at that position. This suggests that the length of the alkyl tail determines the shape of the fiber and also which type of interaction between the single fibers takes place. Generally, a longer alkyl tail hampers crystalline packing, so it is not surprising that the compounds with a longer alkyl tail do not form crystalline knots. A possible explanation for the influence of the molecular structure on the shape of the fibers must lie in the packing inside such a fiber. If the molecules are arranged in an antiparallel fashion, the alkyl tails could all lie in one direction, perpendicular to the long axis of the fiber. Increasing the length of the alkyl tail would increase the cross section of the fiber only in this direction, thus going from a round fiber to a flat one. A schematic representation of a possible molecular model of the fibers is given in Figure 8.

In this model the cholic acid groups are in the core, connected to each other by hydrogen bonds, and the alkyl tails are on the outside. Such a model could explain the aspect ratio of less than one for compounds with longer tails. Probably the changeover occurs around an alkyl tail length of two or three carbon atoms. A remarkable example in this respect is the difference between LeuMe and LeuBu. The only difference is the presence of a methyl group instead of a butyl group, whereas the rest of the molecule is identical, but both compounds form fibers with different shapes and different interactions.

Conclusions

SANS measurements have shown the presence of thin fibers (radius ±10−20 Å) for all studied cholic acid-based organogelators. There are two types of interactions between different single fibers, depending on the molecular

(25) Mittelbach, P.; Porod, G. *Acta Phys. Austr.* **1961**, *14*, 185−211.
(26) de Schepper, I. M. Private communications.

structure of the gelator. Compounds with an alkyl tail of at least four carbon atoms attached to cholic acid, possibly via an amino acid spacer, have loose entanglements between flat fibers. Compounds with only a methyl group at that position have crystalline knots with an average size of 100−200 Å between round fibers. This type of network displays a gradual disintegration upon heating. A large part of the gelator is not taking part in the network, but is freely dissolved.

Acknowledgment. W.G.B. thanks Prof. I. M. de Schepper, Dr. H. Kaya, and Dr. E. Eiser for valuable discussions about the data analysis. The ILL, Grenoble, is acknowledged for providing us with beam time to perform these measurements.

LA035041Y